IEEE Access
Multidisciplinary | Rapid Review | Open Access Journal

Received March 31, 2020, accepted April 9, 2020, date of publication April 14, 2020, date of current version May 5, 2020.

Digital Object Identifier 10.1109/ACCESS.2020.2987807

A Robotic Grinding Motion Planning Methodology for a Novel Automatic Seam Bead Grinding Robot Manipulator

WANJIN GUO[1,2], YAGUANG ZHU[1], (Member, IEEE), AND XU HE[1]
[1]Key Laboratory of Road Construction Technology and Equipment of MOE, Chang'an University, Xi'an 710064, China
[2]State Key Laboratory of Robotics and Systems, Harbin Institute of Technology, Harbin 150001, China

Corresponding author: Yaguang Zhu (zhuyaguang@chd.edu.cn)

This work was supported in part by the Thirteenth Five-Year Plan Equipment Pre-Research Field Fund under Grant 61403120407, in part by the Natural Science Basic Research Plan in Shaanxi Province of China under Grant 2019JQ-426, in part by the State Key Laboratory of Robotics and System (HIT) under Grant SKLRS-2020-KF-08, in part by the Fundamental Research Funds for the Central Universities, CHD, under Grant 300102250104, Grant 300102259308, and Grant 300102259401, and in part by the Shaanxi International Science and Technology Cooperation Project under Grant 2019KW-015.

ABSTRACT Industrial robotics is a continuously developing area of in-depth robotics research, as industrial robots have demonstrated to possess advantages in the robotic automation solutions in the industrial automation applications. In this paper, a novel automatic seam bead grinding robot manipulator with the integration of machining and measuring is proposed and an experimentation platform is developed for the robotic removal of the seam weld beads at welded pipe ends. Also, a robotic grinding motion planning methodology, which consists of a robotic operation process motion planning approach and a robotic seam bead grinding method, is presented for the appropriate motion planning and applications of the operational processes. Furthermore, the effectiveness of the robotic grinding motion planning methodology and the superiorly operational manipulation performance of the proposed robot manipulator are verified through a robotic grinding experiment for the removal of external seam weld beads at a helical welded pipe end.

INDEX TERMS Industrial robotics, grinding robot manipulator, motion planning, seam bead grinding, welded pipe end.

I. INTRODUCTION

Industrial robotics is an area of in-depth robotics research with advanced technology for the variety of industrial automation applications that attracts considerable attention in recent years [1]–[6]. Although the development and application of industrial robots are confined, to a certain extent, to the field of advanced manufacturing due to the lack of stiffness and only withstanding relatively low cutting force of an industrial robot compared to a numerical control machine, the industrial robot, as a commonly available and cost-effective choice, exhibits its own advantages and potentials especially in some applications that require high dexterity adjustment and manipulation performance, large working space, large-sized complex shaped parts and/or operational machining in a wide range. Therefore, industrial robots are extensively invented and introduced into factories for robotic grinding and machining and other applications such as materials handling, spot welding, spray automation and parts assembly. Such robotic automation frees human operators from tedious and tiring labor and such industries rapidly retool their manufacturing lines into robot-integrated systems. Also, these industries make a wide range of manufacturing processes simpler, more functional, intelligent and programmable by offering a real gain of flexibility, scalability, portability, modularity, and access for machining on production lines, and they are feasible alternative solutions for high productivity, quality, and adaptability at minimal cost. Consequently, industrial robotics has exerted an evolutionary impact on the design and operation of manufacturing processes [7]–[15].

In the welded steel line pipe manufacturing, the removal of seam weld beads at helical or longitudinal welded pipe ends is an important process in the industrial welded pipe fabrication,

The associate editor coordinating the review of this manuscript and approving it for publication was Liang Hu.

whose grinding accuracy and quality conformity may exert a crucial influence on the finish requirements of pipe ends and the pressure performance of line pipe couplings. The fabricated welded line pipe aims at the dependable transmission of oil, gas, water and other liquefied media to any type of collection and distribution point.

Currently, the seam weld beads at welded line pipe ends is often removed manually with safety and health risks, or by a belt grinder directly equipped with an industrial robot arm without any other operational motion parts. As a result, the removal quality and accuracy will be unavoidably suffered from adverse effects, due to a low level of the factual accuracy and consistency of the manual removal or the defective nature of the industrial robot arm, such as the weakened structural rigidity of the cantilever-beam-like extended industrial robot arm when it is reaching a far end of the working space, and the small safety margins between industrial robot arm and line pipe resulting from its difficulties in both obstacle avoidance adjustment and grinding orientation adjustment.

However, only a few robot manipulators or robotic machine tools are purposely designed for the removal of seam weld beads of helical welded line pipe ends with automatic processing for the last several years. As a result, the line pipe products manufacturing quality and pipe fabrication efficiency are subject to various constraints and restrictions. Overtime, the demand for robot manipulators dedicated to above mentioned applications has been growing.

Motivated by above reason, a novel automatic seam bead grinding robot manipulator with the integration of machining and measuring, and a robotic grinding motion planning methodology consisting of a robotic operation process motion planning approach and a robotic seam bead grinding method, are proposed for the removal of seam weld beads at pipe ends. Also, an experimentation platform is developed. The main contributions of this paper are given as follows:

(1) The structure design of the robot manipulator and the developed experimentation platform are proposed for the automatic removal of seam weld beads at pipe ends and the weld seam profile measurement.

(2) A robotic operation process motion planning approach is proposed for the operational processes of the automatic removal of seam weld beads at pipe ends.

(3) A robotic seam bead grinding method is proposed for the complete removal of the helical seam weld beads at pipe ends with the proposed robot manipulator.

(4) A seam weld beads removal experiment is conducted on the developed experimentation platform, that demonstrates the grinding performance of the proposed robot manipulator and the effectiveness of the proposed robotic operation process motion planning approach and the proposed robotic seam bead grinding method.

The rest of this paper is organized as follows. Related works are introduced in Section II. The structure and the experimentation platform of the proposed robot manipulator is described in Section III. Forward and inverse kinematics are solved in Section IV. The designed control system of the proposed robot manipulator is presented in Section V. A robotic seam bead grinding method and a robotic operation process motion planning approach are proposed for robotic weld beads removal in Sections VI and VII, respectively. A robotic grinding experiment for the external seam weld beads of a helical welded line pipe is conducted in Section VII. Finally, the conclusion and some future work are given in Section IX.

II. RELATED WORKS

In this section, some related works on robot manipulators or robotic machine tools for robotic grinding applications and the related motion planning are introduced.

Several recent studies were concentrated on robot manipulators or robotic machine tools for robotic grinding applications. A wheel-type in-pipe grinding robot, consisting of a moving structure, a positioning structure, and a grinding structure, was designed to grind girth weld beads for the circular boiler header on the inner walls of pipes [16]. An automatic portable three-axis orbital milling system was designed for removal of degraded dissimilar metal welds in piping systems of the nuclear power plants and preparation of the weld grooves of prescribed geometry for the repair welding [17]. A multi-sensor belt grinding experimentation setup was developed for the automatic endpoint detection and process parameters analysis of the weld seam removal in a robotic abrasive belt grinding process with the help of a vision system [18]–[21]. A rail-grinding car with an open-structured abrasive belt [22] and a other rail grinding device with a closed abrasive belt [23], both including four individual grinding units, were designed for the rail corrugation grinding of high-speed railways. A self-developed belt grinding machine was presented for the robotic abrasive belt grinding of aero-engine blades in the finishing process [24]. An abrasive belt grinding apparatus for the rail grinding was designed, and also the wear mechanisms of abrasive belts in the steel grinding process [25], the influencing mechanism of the rubber wheel on contact pressure and metal removal of the corrugated rail [26] and the effects of the contact pressure and the grinding performance [27] were investigated. An experimentation setup of robotic abrasive belt grinding was presented and a robotic abrasive belt grinding of titanium alloy test workpiece considering the effects of cut-in and cut-off was conducted [28]. A robotic belt grinding experimentation platform was proposed, and a plane grinding experiment and a spline curve contour workpiece surface grinding experiment were carried out [29]. A robotic belt grinding system and a sound-based grinding belt condition monitoring method were presented, and the robotic belt grinding experiments were conducted [30].

Also, several works were concentrated on computer numerical control (CNC) or numerical control (NC) grinding machine tools for grinding tasks. A seven-axes and six-linkage adaptive abrasive belt grinding machine tool was developed and belt grinding experiments of the pure

industrial iron specimens were carried out [31], and also, the physical model for the blisk-blade abrasive belt grinding was built and the grinding vibration mechanism and process parameter optimization for the blisk-blade abrasive belt grinding were investigated [32]. A grinding machine tool was designed and the abrasive belt grinding experiment for blisk specimens was conducted in a thirteen axes computer numerical control abrasive belt grinding machine [33]. A belt grinding mechanism was proposed and several grinding experiments for an aero-engine fan blade were carried out on a five-axis belt grinding machine with flexible grinding mechanism [34]. A five-axis belt grinding machine with integrated functions of measuring and machining was developed, which was mainly composed of gantry structure, belt grinding equipment, measuring devices, rotary table and fixtures, and some belt grinding examples were carried out [35]. A kind of six-axis belt grinding machine tools used for grinding the surface of aero engine blades was presented [36].

There are certain constraints of these reported research works in terms of the robot manipulator or the machine tool for the robotic grinding application. Some of the motion planning of these robot manipulators or robotic machine tools for the workpiece grinding via the robotic abrasive belt grinding depends mainly on the used industrial robot arm, due to the belt grinder equipped only with the end-effector of the industrial robot arm [18]–[21], or the end-effector of the industrial robot arm directly griped the workpiece to take grinding [24], [28]–[30]. Also, the grinding device is designed for the rail corrugation grinding along the longitudinal rail top and it is only suitable for the grinding without operational orientation adjustment [22], [23]. The grinding apparatus is presented only for the experimentation investigation of the influencing mechanism and the grinding performance of the rail material [25]–[27]. The grinding robot is only suitable for grinding girth weld beads on the inner walls of pipes [16], [17]. Moreover, a relatively small accessible workspace of the machine tool can be reached to accomplish grinding tasks [31]–[36].

The motion planning of robotic grinding, detecting seam weld beads or robotic welding were investigated by several recent works. The grinding motion for the robotic grinding and measuring was discussed for the automatic manufacturing process of blade edges [37]. A motion planning algorithm was proposed for the collision-free robot belt grinding through adjusting the machining frame on the belt to implement axial translation along the belt and tangent rotation [38]. The motion planning for dual robots is investigated for the autonomous robotic grinding of intersecting curves [39]. A task-constrained motion planning method was presented for an aerial manipulator to perform non-trivial physical interaction tasks, and detecting and mapping the seam weld beads of the longitudinal welded pipe were demonstrated [40]. An offline motion planning algorithm by considering welding angular redundancy was proposed, which implemented a collision-free motion for the robot welding process by sampling the redundant angular space and considering the position constraints [41]. A motion planning method was proposed to deal with the problem of completing fillet seam welding while turning around the right angle seam simultaneously and provide a reliable theoretical basis for complex all-position welding operations for an all position autonomous welding mobile robot [42]. And a motion planning approach was presented to optimize the obstacle-crossing and the welding model for this robot vehicle and several experiments explained the feasibility of the obstacle-crossing and the continuity of the welding seam [43]. Also, a broken line motion planning was discussed to achieve optimal co-ordination between the respective movement of this robot vehicle and the torch, and optimal control of the mechanical joints and spatial position for broken line welding seams [44].

Only a few robot manipulators or robotic machine tools and their corresponding motion planning were intentionally developed for the automatic seam weld bead grinding at welded steel line pipe ends, which is the main concern of our work. For this purpose, a novel automatic seam bead grinding robot manipulator and a robotic grinding motion planning methodology are specifically investigated, which aim at the removal of seam weld beads of helical welded line pipe ends in automatic processing.

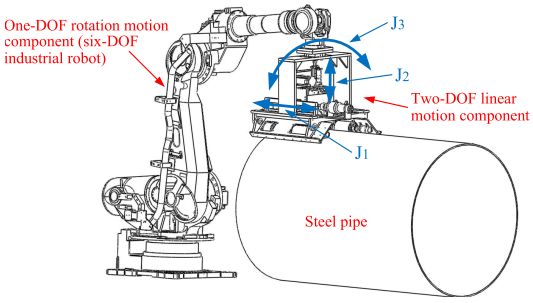

FIGURE 1. Proposed automatic seam bead grinding robot manipulator.

III. STRUCTURE DESCRIPTION AND EXPERIMENTATION PLATFORM

In this section, an automatic seam bead grinding robot manipulator, which integrates machining and measuring, is proposed for the removal of the external and internal seam weld beads (helical or longitudinal welded pipe) at submerged arc welded (SAW) steel line pipe ends. This robot manipulator is an eight-degree-of-freedom (eight-DOF) redundant robot manipulator, and its configuration is 2T6R (here, abbreviated T and R represent the translational motion type and the rotational motion type, respectively; and their joint configurations are the helical joint type (i.e., a ball screw assembly which converts rotary motion to linear motion) and the revolute joint type, respectively). The overall structure of this novel robot manipulator is showed in Fig. 1. The robot manipulator consists of a two-degree-of-freedom (two-DOF) linear motion component (2T) (as shown in Fig. 2) and a six-degree-of-freedom (six-DOF) industrial robot (6R).

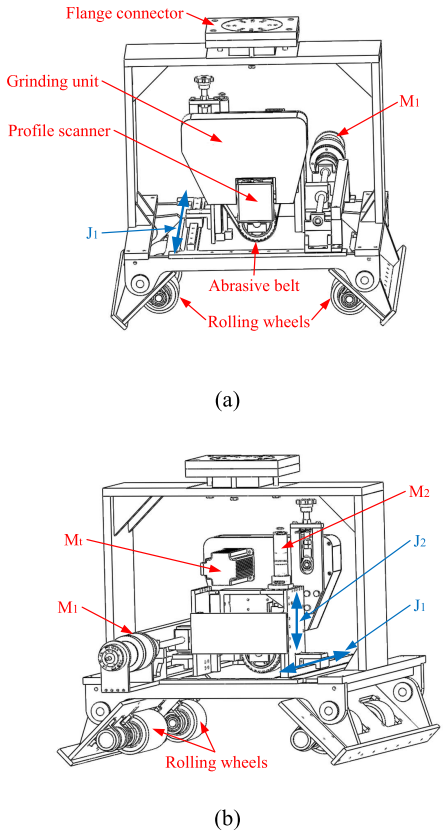

FIGURE 2. Two-DOF linear motion component of proposed robot manipulator.

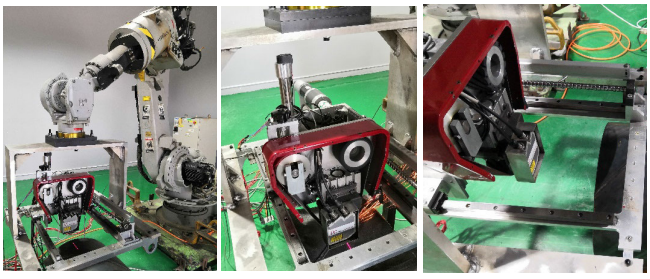

FIGURE 3. Experimentation platform. (a) Overall platform. (b) and (c) two-DOF linear motion component.

The experimentation platform of the robot manipulator is showed in Fig. 3.

The proposed robot manipulator can perform three necessary motions in a decoupled way in the removal process of seam weld beads, i.e., the axial linear motion (J_1), the normal linear motion (J_2), and the circumferential rotation motion (J_3), as shown in Fig. 1 and Fig. 2. The directions of these decoupled motions are defined as the axial direction J_1 (parallel to the longitudinal axis of the pipe), the normal direction J_2 (orthogonal to the axial direction and perpendicular to the surface of the pipe) and the circumferential direction J_3 (along the transverse axis of the pipe), respectively. The motion J_1 and J_2 of this two-DOF linear motion component are decoupled from each other. The six-DOF industrial robot is used to execute the circumferential rotation motion J_3 and adjust the orientation. It is later called the one-degree-of-freedom (one-DOF) rotation motion component in the rest of the paper.

The proposed robot manipulator is dually driven by the two-DOF linear motion component and the one-DOF rotation motion component. The two-DOF linear motion component consists of two sets of ball screws and two pairs of guideway-slider subsystem respectively connected to the rotary DC servo motor M_1 and M_2 that produce the motion J_1 and J_2. The one-DOF rotation motion component is driven by a commercially available six-DOF industrial robot that performs the motion J_3 and adjusts the orientation.

The two-DOF linear motion component is sensor-equipped, including a high-precision three-dimensional (3D) laser-line profile scanner and a grinding unit connected the normal guideway-slider subsystem, which are used as the visual device offering 3D precision measurement and the operational tool making robotic abrasive belt grinding, respectively. Also, the two-DOF linear motion component includes a grating sensor and a magnetic scale sensor, which are used to implement the motion position feedback in axial and normal direction, respectively. The grinding unit includes a high-speed triangular belt (the abrasive grit is 36 mesh) actuated by an alternating-current (AC) servomotor M_t and a cylinder to achieve the weld beads removal with a controlled constant pressure.

The required motions of proposed robot manipulator, i.e., J_1, J_2 and J_3, can be planned separately in a decoupled way. That is, the one-DOF rotation motion component achieves the requirements of large workspace and orientation adjustments, and the two-DOF linear motion component realizes the final fine-tuning of the positioning to achieve the high-precision removal of seam weld bead. In addition, the decoupling of the motion planning allows the manipulator to automatically adapt to the out-of-roundness of pipe and the different pipe diameters.

Benefited from the effective dual drive and motion-decoupled mechanical design, the proposed robot manipulator overcomes the limitations of conventional positioning system, and satisfies the requirements of large travel range, high speed and high accuracy at the same time. Moreover, the weld beads at pipe ends can be removed completely without causing mechanical damage to the steel pipe substrate. The amount of removal can be adjusted in real time according to the obtained actual seam weld bead profiles. Also, the removal height and residual height of weld beads are provided automatically by the visual precision measurement.

The other main mechanical structure features of the proposed robot manipulator includes: (a) adoption of a high-precision 3D profile scanner (which uses the laser line triangulation principle) offering 3D precision measurement to automatically track and detect spatial seam weld bead positions, search for weld bead feature points, conduct 3D reconstruction and carry out the residual height measurement

after the removal of seam weld beads (helical or longitudinal welded pipe) at SAW steel pipe ends; (b) a grinding unit including a high-speed triangular belt and a cylinder is mounted to automatically perform robotic abrasive belt grinding for weld beads removal with a controlled constant pressure; (c) an axial ball–screw-based linear drive with a grating sensor, and a normal ball–screw-based linear drive with a magnetic scale sensor, are used to achieve the position servo closed-loop motion control in both the axial and normal direction motions; (d) a commercially available six-DOF industrial robot (i.e., the so-called one-DOF rotation motion component) is adopted for the uniform motion control in J_3; (e) a long straight rail component with gantry mechanism characteristic features is applied in the axial and normal motions, respectively, which enhances the rigidity of the grinding unit and transfers the majority of the gravity and the grinding force from the grinding unit to the base framework of the two-DOF linear motion component; (f) the robot manipulator has the automatic adjustment adaptability for the roundness differences between the steel pipes, moreover, it has the applicability for the automatic removal of weld beads for different SAW steel pipe ends with manufacturer outer diameter ranging from 508 mm to 1620 mm. As a result, the proposed robot manipulator offers good performance in removal and measurement of the external and internal seam weld beads at SAW steel pipe ends (especially the helical welded pipe ends).

Compared with a general serial 6R industrial robot directly installing a high-speed triangular belt grinding device with only a rotary motion of the abrasive belt, the proposed robot manipulator offers the following particular advantages: (a) the proposed robot manipulator is an eight-DOF redundant robot manipulator with redundant kinematic degrees of freedom of the decoupled two-DOF linear motion component; and this kinematic redundancy not only provides the greater convenience for the motion planning and decoupling control of the removal operation (i.e., the used six-DOF industrial robot only performs the circumferential rotation motion (J_3), and the two-DOF linear motion component produces the rest of the two required linear motions (J_1 and J_2) in a decoupled way), but also increases the level of dexterity that may be used to avoid workspace obstacles, joint limits and singularities; whereas a general serial 6R industrial robot cannot exhibit this kind of superiority; (b) the required three motions (i.e., J_1, J_2 and J_3) are separately driven by different parts of the proposed robot manipulator, the decoupling of motion planning and motion control of seam weld beads removal can be easily achieved; in the case of a general serial 6R industrial robot, the position and orientation adjustments are completely determined by the industrial robot during the removal operation of seam weld beads and its motion planning and motion control are relatively complicated; and (c) only a very single and small arc segment of the required circumferential rotation motion J_3 is produced by the used six-DOF industrial robot, and its position and orientation changes are relatively smooth, continuous, and without uneven variation; also, the grinding force of the removal operation of seam weld beads is first withstood and vibrations are reduced both by the base framework of the two-DOF linear motion component, and then they are transmitted to the used industrial robot; thus, the effects of the undesirable characteristics of the cantilever-beam-like structure and the structural deflects of the used industrial robot are reduced to some extent; whereas a general serial 6R industrial robot possesses the defective nature for the removal operation of seam weld beads, e.g., the weakened structural rigidity of the extended industrial robot when it is reaching far grinding position with a cantilever-beam-like structure, the grinding force to bear directly, and the poor accessibility and small safety margins between industrial robot and steel pipe resulting from its difficulties in both obstacle avoidance adjustment and grinding orientation adjustment.

IV. FORWARD AND INVERSE KINEMATICS

In this section, the forward kinematics and the inverse kinematics for the proposed robot manipulator are described based on the Denavit–Hartenberg method.

TABLE 1. Geometry parameters of robot manipulator.

Joint i	θ_i	d_i	a_i	α_i
1	θ_1	d_1	a_1	$-\pi/2$
2	θ_2	0	a_2	0
3	θ_3	0	a_3	$-\pi/2$
4	θ_4	d_4	0	$\pi/2$
5	θ_5	0	0	$-\pi/2$
6	θ_6	d_6	a_6	$\pi/2$
7	0	d_7	a_7	$-\pi/2$
8	$-\pi/2$	d_8	a_8	0

A. FORWARD KINEMATICS

The Denavit–Hartenberg method is used to conduct the kinematics modeling of the proposed robot manipulator (i.e., the used six-DOF industrial robot and the two-DOF linear motion component). The reference frames are assigned as shown in Fig. 4. The rotation angle about each revolute joint of the used six-DOF industrial robot are expressed by θ_1, θ_2, θ_3, θ_4, θ_5 and θ_6, respectively. The translational stroke along the screw axis of each ball screw assembly of the two-DOF linear motion component in the axial direction and the normal direction are expressed by S_a and S_n, respectively. The geometric parameters of the robot manipulator are listed in Table 1. These variables can be expressed by

$$S_a = (s_a\varphi_a)/(2\pi) \tag{1}$$

$$S_n = (s_n\varphi_n)/(2\pi) \tag{2}$$

where the constants s_a, s_n, φ_a and φ_n represent the pitch and the rotation angle of ball screws in axial and normal

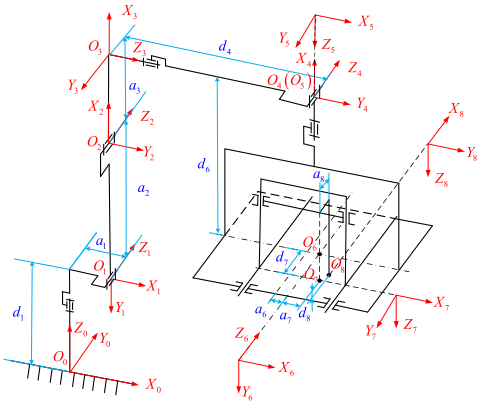

FIGURE 4. Schematic diagram of robot manipulator and assigned reference frames.

directions, respectively. The relationship between translational strokes of ball screws and corresponding geometric parameters of the robot manipulator (Table 1) can be given as

$$S_a = d_7 \tag{3}$$
$$S_n = d_8 \tag{4}$$

According to the assigned reference frames and the actual physical constraints of the used six-DOF industrial robot and the two-DOF linear motion component, the reachable joint ranges are $\theta_1 \in [-\pi, \pi]$, $\theta_2 \in [-3\pi/4, 7\pi/18]$, $\theta_3 \in [-7\pi/6, 4\pi/9]$, $\theta_4 \in [-\pi, \pi]$, $\theta_5 \in [-11\pi/18, 11\pi/18]$ and $\theta_6 \in [-\pi, \pi]$, and the reachable translational stroke ranges of ball screws are $S_a \in [S_{a\_\min}, S_{a\_\max}]$ and $S_n \in [S_{n\_\min}, S_{n\_\max}]$.

It should be noted that the initial angles are $\theta_{2,0} = -\pi/2$ and $\theta_{5,0} = \pi/2$, and other ones are $\theta_{i,0} = 0$ ($i = 1, 3, 4, 6$), based on the assigned reference frames. Thus, the relationship of the actual angle $\theta_{i,a}$ and the calculated angle $\theta_{i,c}$ (i.e., forward and inverse kinematic solutions) of each joint θ_i should be $\theta_{i,a} = \theta_{i,c} + \theta_{i,0}$.

According to the assigned reference frames and the geometry parameters, the homogeneous transformation matrix ${}^{i-1}T_i$ is conducted to represent reference frame *i* relative to frame *i-1*, and it is defined by

$${}^{i-1}T_i = \begin{bmatrix} \cos\theta_i & -\cos\alpha_i \cdot \sin\theta_i & \sin\alpha_i \cdot \sin\theta_i & a_i\cos\theta_i \\ \sin\theta_i & \cos\alpha_i \cdot \cos\theta_i & -\sin\alpha_i \cdot \cos\theta_i & a_i\sin\theta_i \\ 0 & \sin\alpha_i & \cos\alpha_i & d_i \\ 0 & 0 & 0 & 1 \end{bmatrix} \tag{5}$$

where $i = 1, 2, \ldots, 8$, $i \in N$.

In the rest of this paper, several abbreviations are used as $c_i := \cos\theta_i$, $s_i := \sin\theta_i$, $c_{ij} := \cos(\theta_i + \theta_j)$ and $s_{ij} := \sin(\theta_i + \theta_j)$.

The equivalent homogeneous transformation matrix ${}^0T_8$, which relates the spatial displacement of the end-effector reference frame to the base reference frame, can be obtained by successive multiplications of these transformation matrices

$$\begin{aligned} {}^0T_8 &= {}^0T_1\,{}^1T_2\,{}^2T_3\,{}^3T_4\,{}^4T_5\,{}^5T_6\,{}^6T_7\,{}^7T_8 \\ &= \begin{bmatrix} n_x & o_x & a_x & p_x \\ n_y & o_y & a_y & p_y \\ n_z & o_z & a_z & p_z \\ 0 & 0 & 0 & 1 \end{bmatrix} \end{aligned} \tag{6}$$

where

$$\mathbf{p} = [p_x, p_y, p_z]^T \tag{7}$$
$$\begin{aligned} p_x = {} & (c_1c_{23}c_4c_5 - c_1s_{23}s_5 + s_1s_4c_5)\,[c_6\,(a_6 + a_7) \\ & + s_6\,(a_8 + d_7)] - (c_1c_{23}s_4 - s_1c_4)\,[s_6\,(a_6 + a_7) \\ & - c_6\,(a_8 + d_7)] - (c_1c_{23}c_4s_5 + c_1s_{23}c_5 + s_1s_4s_5)\,(d_6 \\ & + d_8) - c_1\,(s_{23}d_4 - a_3c_{23} - a_2c_2 - a_1) \end{aligned} \tag{8}$$
$$\begin{aligned} p_y = {} & (s_1c_{23}c_4c_5 - s_1s_{23}s_5 - c_1s_4c_5) \\ & \times [c_6\,(a_6 + a_7) + s_6\,(a_8 + d_7)] \\ & - (s_1c_{23}s_4 + c_1c_4)\,[s_6\,(a_6 + a_7) - c_6\,(a_8 + d_7)] \\ & - (s_1c_{23}c_4s_5 + s_1s_{23}c_5 - c_1s_4s_5)\,(d_6 + d_8) \\ & - s_1\,(s_{23}d_4 - a_3c_{23} - a_2c_2 - a_1) \end{aligned} \tag{9}$$
$$\begin{aligned} p_z = {} & -(s_{23}c_4c_5 + c_{23}s_5)\,[c_6\,(a_6 + a_7) + s_6\,(a_8 + d_7)] \\ & + s_{23}s_4\,[s_6\,(a_6 + a_7) - c_6\,(a_8 + d_7)] + (s_{23}c_4s_5 \\ & - c_{23}c_5)\,(d_6 + d_8) - c_{23}d_4 - a_3s_{23} - a_2s_2 + d_1 \end{aligned} \tag{10}$$
$$\mathbf{a} = [a_x, a_y, a_z]^T \tag{11}$$
$$a_x = -c_1c_{23}c_4s_5 - c_1s_{23}c_5 - s_1s_4s_5 \tag{12}$$
$$a_y = -s_1c_{23}c_4s_5 - s_1s_{23}c_5 + c_1s_4s_5 \tag{13}$$
$$a_z = s_{23}c_4s_5 - c_{23}c_5 \tag{14}$$
$$\mathbf{o} = [o_x, o_y, o_z]^T \tag{15}$$
$$\begin{aligned} o_x = {} & c_1c_{23}c_4c_5c_6 - c_1s_{23}s_5c_6 + s_1s_4c_5c_6 - c_1c_{23}s_4s_6 \\ & + s_1c_4s_6 \end{aligned} \tag{16}$$
$$\begin{aligned} o_y = {} & s_1c_{23}c_4c_5c_6 - s_1s_{23}s_5c_6 - c_1s_4c_5c_6 - s_1c_{23}s_4s_6 \\ & - c_1c_4s_6 \end{aligned} \tag{17}$$
$$o_z = -s_{23}c_4c_5c_6 - c_{23}s_5c_6 + s_{23}s_4s_6 \tag{18}$$
$$\mathbf{n} = [n_x, n_y, n_z]^T \tag{19}$$
$$\begin{aligned} n_x = {} & c_1c_{23}c_4c_5s_6 - c_1s_{23}s_5s_6 + s_1s_4c_5s_6 + c_1c_{23}s_4c_6 \\ & - s_1c_4c_6 \end{aligned} \tag{20}$$
$$\begin{aligned} n_y = {} & s_1c_{23}c_4c_5s_6 - s_1s_{23}s_5s_6 - c_1s_4c_5s_6 + s_1c_{23}s_4c_6 \\ & + c_1c_4c_6 \end{aligned} \tag{21}$$
$$n_z = -s_{23}c_4c_5s_6 - c_{23}s_5s_6 - s_{23}s_4c_6 \tag{22}$$

B. INVERSE KINEMATICS

As mentioned above, the required three motions (i.e., J_1, J_2 and J_3) in the manufacturing process of the seam weld beads removal are achieved by the completely decoupled motion control of the proposed robot manipulator, i.e., the used six-DOF industrial robot only performs a short arc segment of the circumferential rotation motion (J_3), and the two-DOF linear motion component produces the rest of the two required linear motions J_1 and J_2 in a decoupled way. Thus, the two-DOF linear motion component only needs to

adjust translational strokes of ball screws (i.e., S_a and S_n) based on the set of locations and heights of the seam weld beads. At the same time, the used six-DOF industrial robot only needs to program a very single and short arc segment of the required circumferential rotation motion J_3 through the rotation angles θ_1, θ_2, θ_3, θ_4, θ_5 and θ_6, with the relatively smooth and continuous position and orientation adjustments.

Owing to this decoupled motion adjustments of the proposed robot manipulator, the inverse kinematics consists of two separate parts; one deals with the solutions of translational strokes of ball screws of the two-DOF linear motion component (i.e., S_a and S_n, that is d_7 and d_8, respectively), and the other deals with the solutions of the rotation angles of the used six-DOF industrial robot (i.e., θ_1, θ_2, θ_3, θ_4, θ_5 and θ_6).

1) SOLVING d_7 AND d_8 (THAT IS, S_a AND S_n)

Given any point of the operation task, its representations relative to the base frame (i.e., the frame O_0) can be expressed in terms of the equivalent homogeneous transformation matrix ${}^0T_8$, i.e., the known position ${}^0\mathbf{p}_8$ and orientation ${}^0R_8$ are expressed as

$$ {}^0\mathbf{p}_8 = \left[p_x, p_y, p_z\right]^T \tag{23} $$

$$ {}^0R_8 = [\mathbf{n}, \mathbf{o}, \mathbf{a}] = \begin{bmatrix} n_x & o_x & a_x \\ n_y & o_y & a_y \\ n_z & o_z & a_z \end{bmatrix} \tag{24} $$

The arc segment trajectory of the used six-DOF industrial robot relative to the base frame (i.e., the frame O_0) can be planned independently in advance. Thus, combined with the assigned reference frame O_6, the known position $\mathbf{p}_{arc}$ and orientation R_{arc} of any point on this planned arc segment can be expressed as

$$ {}^0\mathbf{p}_6 = \mathbf{p}_{arc} = [p_a, p_b, p_c]^T \tag{25} $$

$$ {}^0R_6 = R_{arc} = [\mathbf{n}_{arc}, \mathbf{o}_{arc}, \mathbf{a}_{arc}] = \begin{bmatrix} n_a & o_a & a_a \\ n_b & o_b & a_b \\ n_c & o_c & a_c \end{bmatrix} \tag{26} $$

Based on the assigned reference frames O_6, O_7 and O_8, and the homogeneous transformation matrix ${}^6T_7$ and ${}^7T_8$, giving

$$ S_a = d_7 = p_c - p_x - a_8 \tag{27} $$

$$ S_n = d_8 = p_b - p_z \tag{28} $$

$$ \mathbf{n}_{arc} = \mathbf{o} \tag{29} $$

$$ \mathbf{o}_{arc} = \mathbf{a} \tag{30} $$

$$ \mathbf{a}_{arc} = \mathbf{n} \tag{31} $$

2) SOLVING θ_1, θ_2, θ_3, θ_4, θ_5 AND θ_6

Based on the homogeneous transformation matrix ${}^{i-1}T_i$ $(i = 1, 2, \ldots, 6, i \in N)$, yielding

$$ \theta_1 = \arctan 2\left(w_y/(a_3c_{23} + a_2c_2 + a_1 - s_{23}d_4),\right. \\ \left. w_x/(a_3c_{23} + a_2c_2 + a_1 - s_{23}d_4)\right) \tag{32} $$

where

$$ w_x = p_a - n_a a_6 - o_a d_6 \tag{33} $$

$$ w_y = p_b - n_b a_6 - o_b d_6 \tag{34} $$

where the arctan 2 function is the four quadrant arctangent function, e.g., $\arctan 2\,(Y, X) = \arg\,(X + jY) \in (-\pi, \pi]$, $j = \sqrt{-1}$, i.e., it returns the argument of the complex number with real part X and imaginary part Y.

Also, other rotation angles can be obtained as

$$ \theta_2 = \arctan 2\,(l_3, l_4) + \arctan 2\,(l_2, l_1) \tag{35} $$

or

$$ \theta_2 = \arctan 2\,(l_3, -l_4) + \arctan 2\,(l_2, l_1) \tag{36} $$

$$ \theta_3 = \arctan 2\,(l_1 + a_2s_2, l_2 - a_2c_2) \\ - \arctan 2\,(d_4, a_3) - \theta_2 \tag{37} $$

where

$$ l_1 = d_1 - (p_c - n_c a_6 - o_c d_6) \tag{38} $$

$$ l_2 = w_x c_1 + w_y s_1 - a_1 \tag{39} $$

$$ l_3 = \left(d_4^2 + a_3^2 - a_2^2 - l_1^2 - l_2^2\right)/\left(2a_2\sqrt{l_1^2 + l_2^2}\right) \tag{40} $$

$$ l_4 = \sqrt{1 - l_3^2} \tag{41} $$

Case 1: $\theta_5 \neq 0$.

If $c_4\,(o_a c_1 c_{23} + o_b s_1 c_{23} - o_c s_{23}) > 0$ or $s_4\,(o_a s_1 - o_b c_1) > 0$, then

$$ \theta_5 = \arccos\,(-o_a c_1 s_{23} - o_b s_1 s_{23} - o_c c_{23}) \tag{42} $$

and if $c_4\,(o_a c_1 c_{23} + o_b s_1 c_{23} - o_c s_{23}) < 0$ or $s_4\,(o_a s_1 - o_b c_1) < 0$, then

$$ \theta_5 = -\arccos\,(-o_a c_1 s_{23} - o_b s_1 s_{23} - o_c c_{23}) \tag{43} $$

and

$$ \theta_4 = \arctan 2\,((o_b c_1 - o_a s_1)/s_5, \\ (o_c s_{23} - o_a c_1 c_{23} - o_b s_1 c_{23})/s_5) \tag{44} $$

$$ \theta_6 = \arctan 2\,((-a_a c_1 s_{23} - a_b s_1 s_{23} - a_c c_{23})/s_5, \\ (-n_a c_1 s_{23} - n_b s_1 s_{23} - n_c c_{23})/s_5) \tag{45} $$

Case 2:$\theta_5 = 0$.

In this case, θ_4 takes its last solution, and

$$ \theta_6 = \arctan 2\,(a_a c_1 c_{23} + a_b s_1 c_{23} - a_c s_{23}, \\ n_a c_1 c_{23} + n_b s_1 c_{23} - n_c s_{23}) - \theta_4 \tag{46} $$

It should be noted that there may be multiple inverse kinematic solutions of the used six-DOF industrial robot, which need to be determined according to the reachable range, and the continuity of the solutions must be ensured.

V. CONTROL SYSTEM

A specially designed control system is essential for the performance and compliance of a robotic system. In this section, the hardware and software architecture of the control system for the two-DOF linear motion component of the proposed robot manipulator is presented.

The robot communication software MOTOCOM32 (which is manufactured by the robot manufacturer YASKAWA) is used to achieve the communication transmission between the two control systems (i.e., the designed control system of the two-DOF linear motion component, and the industrial robot controller of the used six-DOF industrial robot).

The designed control system for the two-DOF linear motion component is built based on NI PXI-7358 motion controller and Laboratory Virtual Instrument Engineering Workbench (LabVIEW). The former is a programmable multi-axis motion control card with the peripheral component interconnect (PCI) extensions for instrumentation bus (i.e., PXI bus). The latter provides a system-design platform and an application development environment with interactive graphics features to develop a control system and create motion control applications.

The hardware of the designed control system consists of two parts; one deals with the motion control and motion trajectory generation through the motion controller (NI PXI-7358), the PXI express embedded controller (NI PXIe-8821), the PXI express-compatible chassis (NI PXIe-1071) and the motion interface (NI UMI-7774), here, combining the PXIe-8821 embedded controller with the PXIe-1071 PXI express-compatible chassis, results in a fully PC-compatible computer in a compact and rugged package; and the other deals with the seam weld beads identification and detection, the position feedback, the seam weld beads removal operation, etc. by the 3D profile scanner, the DC servo driver, the grating sensor, the magnetic scale sensor and the AC servo amplifier.

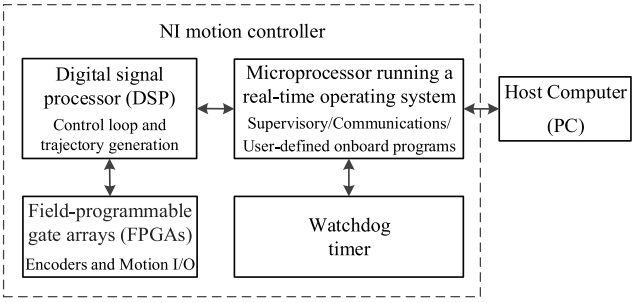

FIGURE 5. Physical NI motion controller architecture (NI PXI-7358).

Among them, the core hardware component of the control system is the NI PXI-7358 motion controller. Together with the NI PXIe-8821 PXI express embedded controller, both are installed inside the express chassis (NI PXIe-1071) and connected with the motion interface (NI UMI-7774). The physical architecture of the NI PXI-7358 motion controller hardware is illustrated in Fig. 5. The typical functional architecture components of the NI PXI-7358 motion controller are shown in Fig. 6.

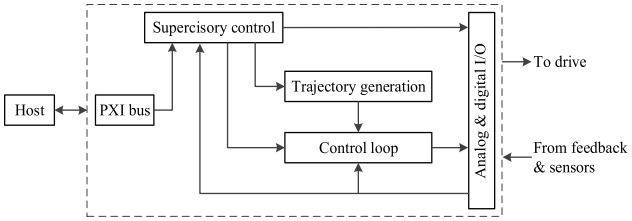

FIGURE 6. Typical NI motion controller functional architecture (NI PXI-7358).

The main functions of the other hardware components of the designed control system are described briefly below. The 3D profile scanner acquires data for graphing and tracking purposes, i.e., it performs the automatic motion tracking and detection, and the residual height measurement for seam weld beads at SAW steel pipe ends. The DC servo driver, the grating sensor and the magnetic scale sensor handle the position closed-loop feedback control of DC servo motors for the axial motion and normal motion of the proposed robot manipulator. The AC servo amplifier controls the AC servo motor driving for the grinding unit to automatically perform robotic abrasive belt grinding for weld beads removal.

The software of the designed control system is built directly on the LabVIEW, which offers a system-design platform and application development environment and uses a graphical programming language named G featuring interactive graphics, so that the required control flow can be programmed using a graphic interface. The LabVIEW also provides an integrated development environment (IDE), including debugging, automated multithreading, application user interface, hardware management and interface for system design. In order to provide easy communication and programming of the NI PXI-7358 motion controller, the NI-Motion driver software is utilized to provide a set of powerful high-level software commands through the comprehensive application programming interface (API).

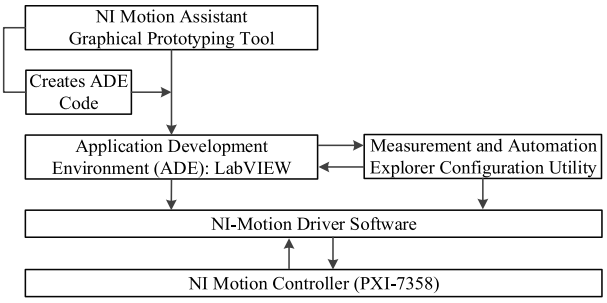

FIGURE 7. Motion control interaction between hardware and software.

In this paper, the motion control interaction between the hardware and the software of the designed control system for the two-DOF linear motion component is shown in Fig. 7. The generic steps are required to design a motion application and

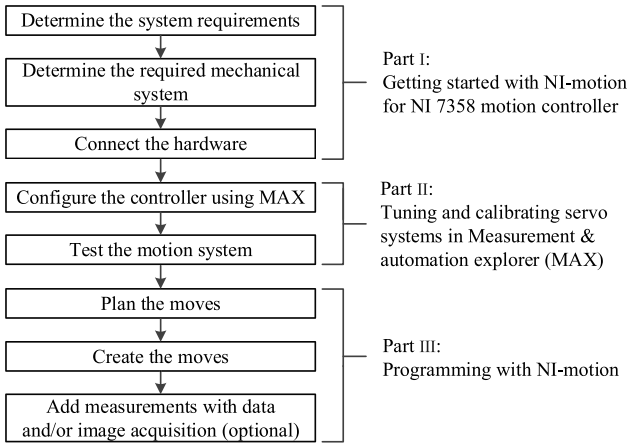

FIGURE 8. Generic steps for designing a motion application.

the steps for creating an application with NI-Motion using the NI 7358 controller are described in Fig. 8.

VI. ROBOTIC SEAM BEAD GRINDING METHOD

In this section, a robotic seam bead grinding method for the helical seam weld beads at SAW steel pipe ends is proposed. This proposed method offers a complete removal process of the helical seam weld beads at welded pipe ends. The detailed description of this method is presented in the following steps.

Step 1. Initialize the system and do self-checking for the proposed robot manipulator.

Step 2. Bring the robot manipulator to the home position and identify the pipe arriving at the specified position (the home position is also regarded as the zero position in an absolute position frame of reference).

Step 3. Determine the outer diameter of the steel pipe to be removed in the operator interface, find the center position and the highest position of the pipe cross section in the used industrial robot frame of reference through the 3D profile scanner acquiring data from two different points on the pipe surface (which is achieved by the used industrial robot moving from a certain location to other location), and then carry out the trajectory planning of the used industrial robot for the appropriate uniform motion J_3 based on the outer diameter and this found highest position of the pipe cross section.

Step 4. Find the accurate pipe end face and locate the exact position of the pipe end through the visual detection of the 3D profile scanner (which is achieved by the used industrial robot moving along the longitudinal axis of the pipe).

Step 5. Determine the starting point of the helical seam bead grinding (it is also the initial position of the helical seam weld beads to be detected and subsequently removed) by executing two sequential procedures: one reaches a certain position with the specified distance from the pipe end face to this identified position along the longitudinal axis of the pipe; the other deals with the positioning and graphing purposes to be consistent between the marker point of the helical seam weld bead and the visual center of the 3D profile scanner by rotating the pipe around the central axis of the pipe. This identified position on the helical seam weld beads is taken as the starting point of the helical seam bead grinding, and the whole helical seam weld beads to be detected and removed is a spatial curve segment between the starting point and the end point of the helical seam weld beads at the pipe end.

Step 6. Acquire data for graphing and tracking purposes from 3D profile scanner, which is achieved by the coordinated motions J_3 and J_1 in a decoupled way between the used industrial robot and the two-DOF linear motion component; and proceed to the weld beads identification, features identification and the tracking of the helical seam weld beads to be removed along the spatial curve segment. Here, the data saved during the feature identification process include the highest point, the marker point, and the left and right weld toe points of the seam weld beads. Also, the real-time positions of the axial direction of the two-DOF linear motion component are recorded.

Step 7. Make spatial curve fitting, 3D reconstruction and removal planning for the tracked helical seam weld beads.

Step 8. Remove the helical seam weld beads by applying a constant grinding pressure on the grinding unit and do the real-time adjustments of the removal control based on the previous removal planning, which is achieved by the coordinated motions J_1, J_2 and J_3 in a decoupled way.

Step 9. Measure the residual height of the removed helical seam weld beads through the 3D profile scanner (similar to the Step 6).

Step 10. Judge whether the residual height meets the removal requirements. If the residual height meets the given removal requirements, go to Step 11. Otherwise, repeat Step 7-9.

Step 11. Accomplish the removal of the helical seam weld beads at the operational pipe end, and reset the robot manipulator to the home position.

Step 12. Either wait for the arrival of the next pipe end and continue (go back to Step 2), or finish the work on the current helical seam weld beads and stop the robot manipulator.

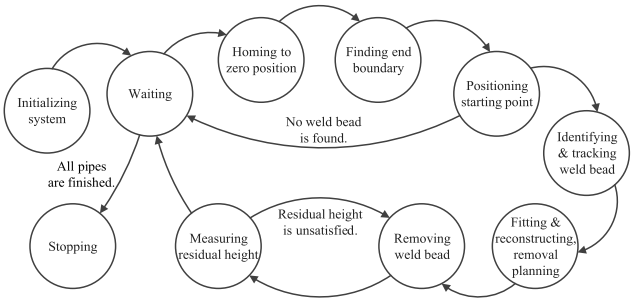

FIGURE 9. State-action-state transition patterns.

The above entire process of the proposed robotic seam bead grinding method can be mainly segmented into a sequence of state-action-state transition patterns based on finite-state machines, as shown in Fig. 9. The feature identification points

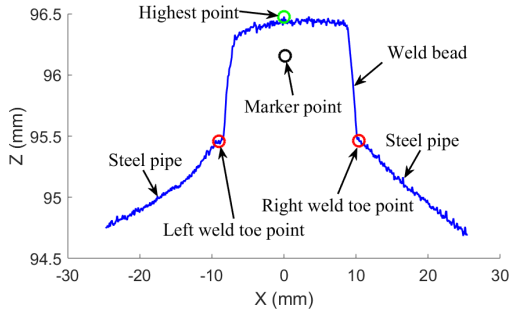

FIGURE 10. Feature identification points of seam weld bead profile.

of the seam weld bead profile in the section along the axial direction of the steel pipe are illustrated in Fig. 10.

Note that the proposed robotic seam bead grinding method is especially suitable for the removal of the helical seam weld beads at welded pipe ends, as well as for the simpler scenario of removing the longitudinal seam weld beads.

VII. ROBOTIC OPERATION PROCESS MOTION PLANNING APPROACH

The helical seam weld beads to be removed is a spatial curve segment on the SAW steel line pipe end and corresponding specifications vary greatly. The manufacturer-designated outer diameter of steel pipe ranges from 508 mm to 1620 mm. The helical angle of the weld seam (which is the constant angle between the tangent to the helical weld seam and a line perpendicular to the axis of the pipe) ranges from 45° (degrees) to 70°. The maximum weld bead width is 25 mm, and the maximum weld bead height is 3.5 mm. The wall thickness of steel pipe ranges from 6 mm to 25.4 mm. The maximum radial offset of strip/plate edges of SAW pipe is 2.5 mm. The maximum steel grade of steel pipe is X100.

Based on the line pipe specification, the following requirements need to be applied to the removal of external weld beads at pipe ends: (a) for a distance of at least 150 mm (6.0 in.) from each pipe end, the external weld bead shall be removed by grinding so that it does not extend above the adjacent pipe surface by more than 0.5 mm (0.020 in.), and (b) the external weld bead shall blend in smoothly with the adjacent pipe surface. Here, the term ''shall'' denotes a minimum requirement in order to conform to the applicable standard.

Taking into account these different product specifications and irregular weld bead characteristics, the motion planning in various processes, including the processes of positioning and tracking, removal of weld beads, residual height measuring, and repeated removal, is an important part of achieving automatic and effective removal operation for the proposed robot manipulator. In this section, a robotic operation process motion planning approach is proposed to achieve the effectiveness of the removal and measurement operations in these four major processes in a completely decoupled motion planning way, which is presented in subsequent parts.

A. ROBOTIC OPERATION OF POSITIONING AND TRACKING

In the process of the positioning and tracking, the main purpose is to position and track the helical seam weld beads, and record the axial motion positions and feature data of weld beads. The motion planning of the two-DOF linear motion component and the one-DOF rotation motion component of the proposed robot manipulator (i.e., the axial, normal and circumferential direction motions J_1, J_2 and J_3) are proceeded as follows: (a) the rotation motion component adopts the uniform motion at a specified speed according to a pre-planned arc trajectory (which is planned based on the specified outer diameter of the steel pipe to be removed and the center position and highest position of the pipe cross section calculated from the 3D profile scanner acquired data) in J_3; (b) the axial linear motion component utilizes position closed-loop-based straight-line move in a given time period in J_1 (which is achieved by the periodic linear motion adjustment to keep coincident between the marker point of the weld bead profile and the scanning center point of the 3D profile scanner); the axial linear motion positions are recorded in a specified time period; and also the data of the weld beads feature identification process are saved in the same specified time period, including the highest point, the marker point, and the left and right weld toe points; (c) the normal linear motion component is located at the specified scanning position and stays stationary in J_2.

B. ROBOTIC REMOVAL OPERATION

During the removal process, the main target is to make the weld beads remove completely by the grinding unit through the coordinated motion of the proposed robot manipulator. The motion planning of the two-DOF linear motion component and the one-DOF rotation motion component are implemented as follows: (a) the rotation motion component also uses the uniform motion at the same specified speed on the basis of the same pre-planned arc trajectory in J_3; (b) the axial linear motion component also utilizes the position closed-loop-based straight-line move in a given time period in J_1, which uses the recorded axial linear motion positions in the process of the positioning and tracking; (c) the normal linear motion component also makes use of the position closed-loop-based straight-line move in the same given time period in J_2 (which uses the calculated weld bead height from the saved feature data in the process of the positioning and tracking).

C. ROBOTIC OPERATION OF RESIDUAL HEIGHT MEASURING

In the process of the residual height measuring, the main goal is to make the residual height measurement after the removal. The motion planning of the two-DOF linear motion component and the one-DOF rotation motion component that both are presented the same manner as the process of the positioning and tracking.

D. ROBOTIC REPEATED REMOVAL OPERATION

The repeated removal operation is needed if the results of the residual height measuring cannot satisfy the specified weld beads removal requirements. In the process of the repeated removal operation, the motion planning of the two-DOF linear motion component and the one-DOF rotation motion component that both are performed the same manner as the removal process.

VIII. ROBOTIC GRINDING EXPERIMENT

The robotic grinding experiment for the external seam weld beads at a helical welded pipe end is conducted on the experimentation platform of the proposed robot manipulator in this section to show the effectiveness of the proposed robotic operation process motion planning approach and the proposed robotic seam bead grinding method, and also to demonstrate the superiority of the operational manipulation performance and the grinding ability of the proposed robot manipulator.

In the robotic grinding experiment, the following specified requirements for the removal of external weld beads at the line pipe end that need to be satisfied: (a) for a distance of at least 150 mm from each pipe end, the external weld bead shall be removed by grinding such that it does not extend above the adjacent pipe surface by more than 0.3 mm, and (b) the external weld bead after removal shall blend in smoothly with the adjacent pipe surface. Note that the requirement of the removed weld bead at pipe end does not extend above the adjacent pipe surface by more than 0.5 mm according to the line pipe specification, and the specified requirement is 0.3 mm in this robotic grinding experiment.

FIGURE 11. Actual outward appearance of spatial helical seam weld beads at steel pipe end.

The manufacturer-designated outer diameter of the experimental helical welded pipe is 508 mm. The actual outward appearance of the helical seam weld beads at the pipe end is showed in Fig. 11. This helical seam weld beads to be removed is a spatial curve segment on the cylindrical surface of the welded steel pipe at the pipe end, as shown in Fig. 12 (here, the Z axis is parallel to the axis of the steel pipe). In the robotic grinding experiment, the end point of the helical seam weld beads segment at the pipe end, and the starting point is located on the pipe surface with a specified distance (180 mm), as shown in Fig. 12.

The experimental arc trajectory of the used six-DOF industrial robot for the appropriate uniform motion J_3 of the proposed robot manipulator is planned as shown in Fig. 13,

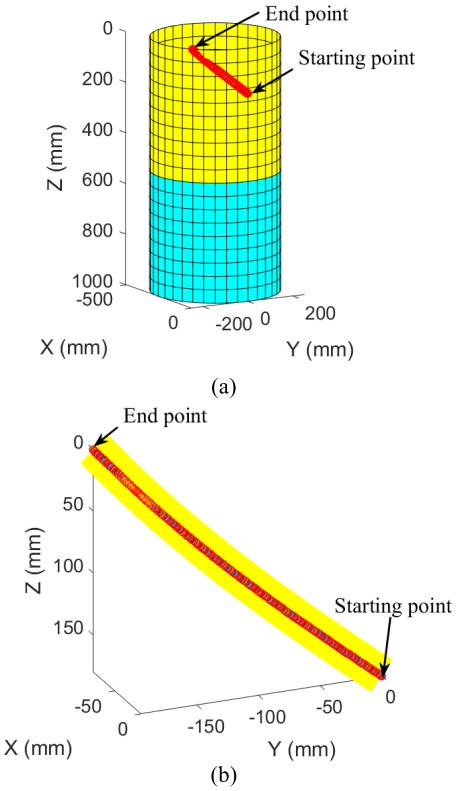

FIGURE 12. Helical seam weld beads on cylindrical surface of welded steel pipe end. (a) Seam weld beads to be removed and welded steel pipe. (b) Seam weld beads to be removed.

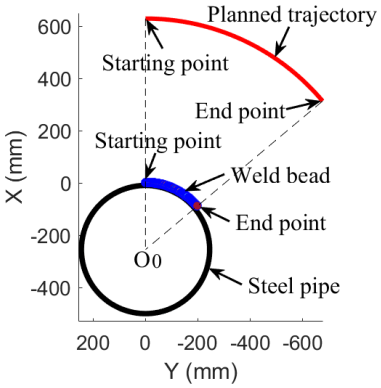

FIGURE 13. Planned circumferential motion trajectory of used six-DOF industrial robot.

based on the outer diameter (508 mm) of the experimental steel pipe and the calculated center- and highest-position of the pipe cross section in the industrial robot frame of reference. This planned trajectory is a plane arc segment in the x–y-plane, and it is along the circumferential direction J_3 (that is, the red arc segment is showed in Fig. 13), which is utilized in above mentioned four major processes. Here, the center- and highest-position are obtained by calculating the outer diameter value and two different point positions on the surface of the experimental steel pipe (these two different point positions are obtained from the visual detection of the 3D profile scanner).

The experimental positioning, tracking and 3D measurement for the whole spatial curve segment of the helical seam

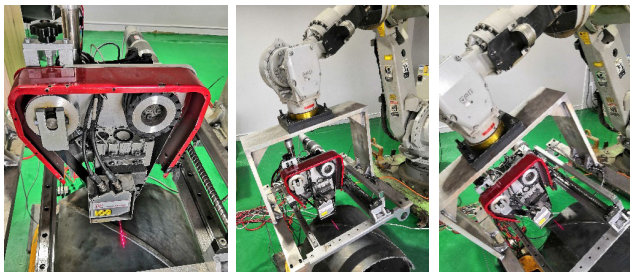

FIGURE 14. Experimental weld beads tracking and features identification.

weld beads at pipe end through the 3D profile scanner is conducted as shown in Fig. 14, which is achieved by moving along J_1 and by moving along the pre-planned uniform motion J_3. The line speed of the used six-DOF industrial robot is 4 mm/s. Here, the projected laser line of the 3D profile scanner is along J_2.

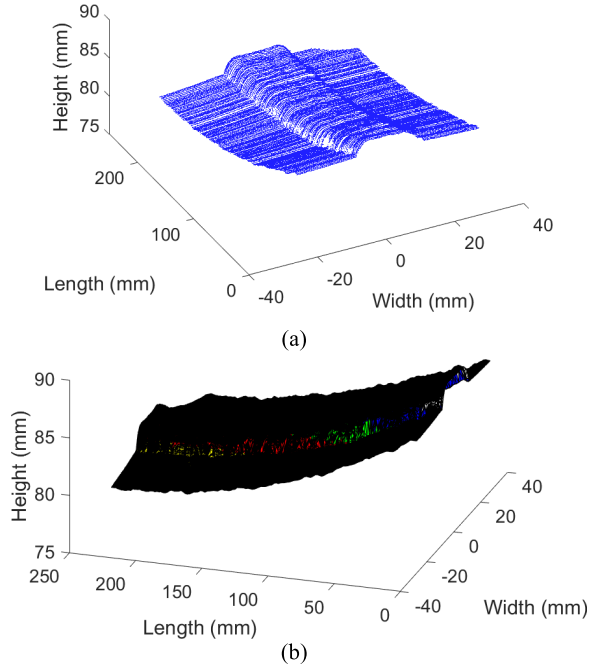

FIGURE 15. Experimental measurement data of helical seam weld beads to be removed at steel pipe end. (a) 3D weld bead profiles. (b) 3D weld bead surface.

The 3D measurement data for the helical seam weld beads by the 3D profile scanner are showed in Fig. 15. A certain sampled profile for the equidistant arrangement of the 3D profile scanner x-z data and the obtained feature identification points, including the highest point, the marker point, and the left and right weld toe points of the seam weld beads, are showed in Fig. 16. The experimental profile height of the helical seam weld beads to be removed is showed in Fig. 17, which corresponds to the maximum removal height of each group along the helical seam weld beads for the sampled 3D measurement data.

Through calculation, the maximum profile height, the minimum profile height, the mean profile height, the standard deviation of the profile height and the variance profile

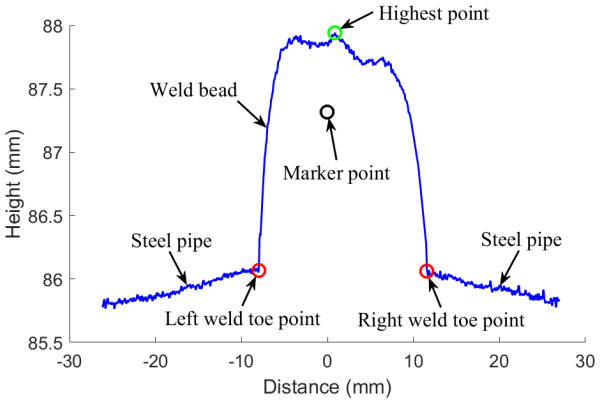

FIGURE 16. Feature identification points of a certain sampled seam weld bead profile.

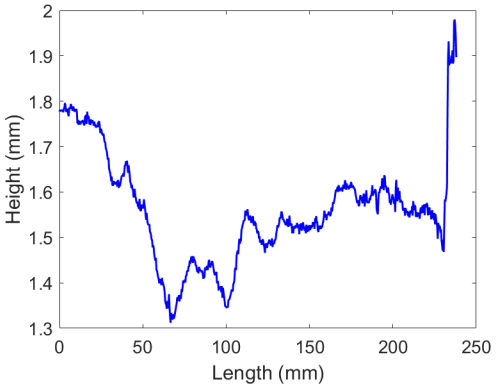

FIGURE 17. Experimental profile height of helical seam weld beads to be removed at steel pipe end.

height are obtained as 1.9800 mm, 1.3120 mm, 1.5591 mm, 0.1210 mm and 0.0146 mm^2, respectively. As shown in Fig. 17, the area with the relatively larger height is located at the end of the helical seam weld beads. This is because the deformation effect on the end of the helical seam weld beads caused by the segmented steel pipe cutting at the steel pipe end face. In general, there is no noticeable difference among the profile height of the helical seam weld beads between adjacent locations.

The spatial curve fitting, 3D reconstruction and removal planning for the helical seam weld beads to be removed at pipe end are conducted simultaneously based on the sampled 3D measurement data. Among them, the removal planning mainly includes: (a) the removal control adjustment planning, which uses the obtained feature identification points and the calculated experimental profile heights; (b) the circumferential, axial, and normal directions (i.e., J_3, J_1 and J_2) motion planning, which uses the pre-planned trajectory of the used six-DOF industrial robot, the sampled recorded positions in the axial direction, and the obtained feature identification points during the feature identification process, respectively; (c) the controlled constant grinding pressure and the controlled constant rotational speed of the robotic abrasive belt grinding unit.

Subsequently, the complete removal of the helical seam weld beads at pipe end is performed according to the previous

FIGURE 18. Robotic grinding of helical seam weld beads at steel pipe end.

removal planning, as shown in Fig. 18. Here, the used controlled constant grinding pressure is 0.55 MPa; the used controlled constant rotational speed of the robotic abrasive belt grinding unit is 3000 revolutions per minute (rpm), and the linear velocity of the abrasive belt is 15.708 m/s; the used adjustment time period is 100 millisecond (ms) for the real-time implementations of the removal control adjustments and motion control in the axial, normal, and circumferential motions; the used line speed of the uniform motion in the circumferential direction is 4 mm/s. The actual robotic grinding result of the helical seam weld beads at pipe end is showed in Fig. 19.

FIGURE 19. Robotic grinding result of helical seam weld beads at steel pipe end.

In order to check the weld beads removal quality and provide measurement data of the residual seam weld beads for future removal process, the residual height measuring for the removed seam weld beads is carried out in a manner that is similar to the process of the experimental positioning, tracking and 3D measurement, as shown in Fig. 20. The 3D measurement data of the profile scanner for the residual seam weld beads after the removal is showed in Fig. 21. The residual profile height of the helical seam weld beads after the removal is showed in Fig. 22, which corresponds to the maximum residual height of each group along the removed seam weld beads for the sampled 3D measurement data.

The residual height measuring results should be given dedicated attention in computational analysis. Through calculation, the maximum residual height, the minimum residual height, the mean residual height, the standard deviation of the residual height and the variance residual height are obtained as 0.2590 mm, 0.0870 mm, 0.1847 mm, 0.0436 mm and 0.0019 mm^2, respectively. It shows that all residual heights of the removed seam weld beads meet the requirement of

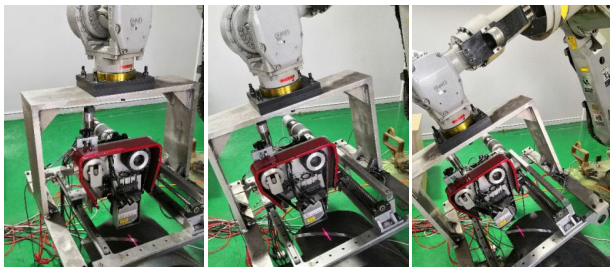

FIGURE 20. Measuring residual height of removed helical seam weld beads at steel pipe end.

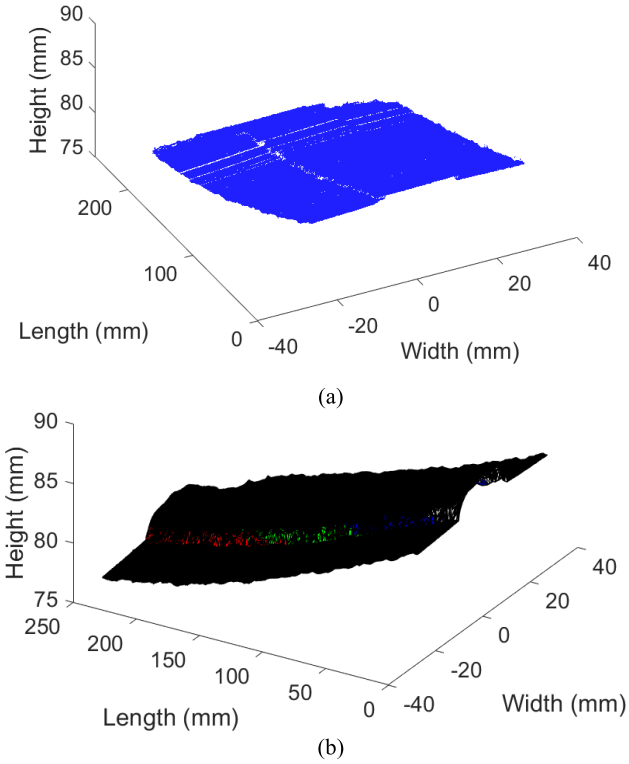

FIGURE 21. Experimental measurement data of residual height after removal of helical seam weld beads at steel pipe end. (a) 3D weld bead profiles. (b) 3D weld bead surface.

the height value between the removed seam weld bead and its adjacent pipe surface (i.e., the aforementioned specified height value is no more than 0.3 mm). Also, the removed seam weld beads are, to a large extent, blended in smoothly with the adjacent pipe surface, without cutting into the parent pipe, as shown in Fig. 19, Fig. 21 and Fig. 22.

Moreover, the actual removal distance between the starting point and the end point along the longitudinal axis of the welded pipe is 180 mm, and this removal distance fulfills the specified distance requirement (i.e., the aforementioned specified distance to be removed by grinding is at least 150 mm).

These residual height measuring results indicates that the removed seam weld beads satisfy the specified requirements for the removal of external weld beads at pipe end. Hence, there is no need for further actions.

It takes 48.29 seconds in each process of the experimental positioning, tracking and 3D measurement, the experimental

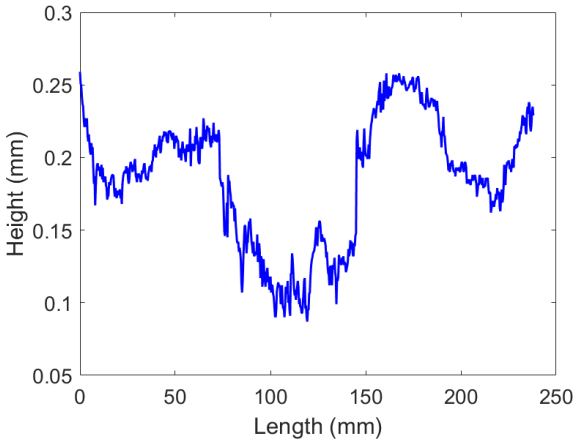

FIGURE 22. Experimental profile height of residual height after removal of helical seam weld beads at steel pipe end.

complete removal, and the residual height measuring. And it takes a total of 218.35 seconds in the entire process of the robotic grinding experiment, including the time cost of initializing system and self-checking of the proposed robot manipulator, finding the accurate pipe end face and locating the exact position of the steel pipe, determining the starting point of the helical seam weld beads to be removed, and homing to the zero position of the robot manipulator.

The above experimental results demonstrate that the experimental removed helical seam weld beads can be able to meet all the requirements and specifications for the removal of weld beads at pipe end as mentioned previously. Also, the effectiveness and the applicability of the proposed robotic operation process motion planning approach and the proposed robotic seam bead grinding method are verified experimentally and they can be able to satisfy the needs of the robotic grinding for the removal of the seam weld beads of the helical welded pipe at pipe end. Moreover, the superiorly operational manipulation performance and the grinding ability of the proposed robot manipulator, which are benefited from the particularly mechanical structure features, are fully demonstrated in the robotic grinding experiment.

IX. CONCLUSION

A novel automatic seam bead grinding robot manipulator with the integration of machining and measuring was proposed and an experimentation platform was developed for the removal of seam weld beads at steel line pipe ends. Also, a robotic grinding motion planning methodology, consisting of a proposed robotic operation process motion planning approach and a proposed robotic seam bead grinding method, was presented for the motion operations and the complete removal processes. Furthermore, the effectiveness of the proposed robotic operation process motion planning approach and the proposed robotic seam bead grinding method was verified through a robotic grinding experiment on the developed experimentation platform. The superiorly operational manipulation performance and the grinding ability of the proposed robot manipulator were also demonstrated in the grinding experiment. The forward and inverse kinematics and the designed control system of the proposed robot manipulator were also presented.

In future work, several meaningful attempts need to be carried out, such as influencing mechanism of the removal of seam weld beads removal, robotic grinding condition monitoring, and further structural improvement of the proposed robot manipulator. The two proposed methods are expected to provide some insight into the foundational aspects of operation process motion planning and seam bead grinding.

ACKNOWLEDGMENT

The authors would like to thank Shaanxi Dai AI Meng De Electronic Technology Co., Ltd., for the help in part of the grinding experiment of this article.

REFERENCES

[1] H. N. Huynh, H. Assadi, E. Riviere-Lorphevre, O. Verlinden, and K. Ahmadi, "Modelling the dynamics of industrial robots for milling operations," *Robot. Comput.-Integr. Manuf.*, vol. 61, Feb. 2020, Art. no. 101852.

[2] M. Kyrarini, M. A. Haseeb, D. Ristire-Durrant, and A. Gräser, "Robot learning of industrial assembly task via human demonstrations," *Auto. Robots*, vol. 43, no. 1, pp. 239–257, Jan. 2019.

[3] J. Sanchez, J.-A. Corrales, B.-C. Bouzgarrou, and Y. Mezouar, "Robotic manipulation and sensing of deformable objects in domestic and industrial applications: A survey," *Int. J. Robot. Res.*, vol. 37, no. 7, pp. 688–716, Jun. 2018.

[4] C. Garriz and R. Domingo, "Development of trajectories through the Kalman algorithm and application to an industrial robot in the automotive industry," *IEEE Access*, vol. 7, pp. 23570–23578, 2019.

[5] Y. Zhang, W. Zhu, and A. Rosendo, "QR code-based self-calibration for a fault-tolerant industrial robot arm," *IEEE Access*, vol. 7, pp. 73349–73356, 2019.

[6] H. Zhang, Y. Wang, J. Zheng, and J. Yu, "Path planning of industrial robot based on improved RRT algorithm in complex environments," *IEEE Access*, vol. 6, pp. 53296–53306, 2018.

[7] S. H. Kim, E. Nam, T. I. Ha, S.-H. Hwang, J. H. Lee, S.-H. Park, and B.-K. Min, "Robotic machining: A review of recent progress," *Int. J. Precis. Eng. Manuf.*, vol. 20, no. 9, pp. 1629–1642, Sep. 2019.

[8] W. Ji and L. Wang, "Industrial robotic machining: A review," *Int. J. Adv. Manuf. Technol.*, vol. 103, nos. 1–4, pp. 1239–1255, Jul. 2019.

[9] B. Tao, X. Zhao, and H. Ding, "Mobile-robotic machining for large complex components: A review study," *Sci. China Technol. Sci.*, vol. 62, no. 8, pp. 1388–1400, Aug. 2019.

[10] L. Yuan, Z. Pan, D. Ding, S. Sun, and W. Li, "A review on chatter in robotic machining process regarding both regenerative and mode coupling mechanism," *IEEE/ASME Trans. Mechatronics*, vol. 23, no. 5, pp. 2240–2251, Oct. 2018.

[11] D.-H. Kim, T. J. Y. Kim, X. Wang, M. Kim, Y.-J. Quan, J. W. Oh, S.-H. Min, H. Kim, B. Bhandari, I. Yang, and S.-H. Ahn, "Smart machining process using machine learning: A review and perspective on machining industry," *Int. J. Precis. Eng. Manuf.-Green Technol.*, vol. 5, no. 4, pp. 555–568, Aug. 2018.

[12] I. Iglesias, J. E. Ares, C. Gonzalez-Gaya, F. Morales, and V. F. Rosales, "Predictive methodology for dimensional path precision in robotic machining operations," *IEEE Access*, vol. 6, pp. 49217–49223, 2018.

[13] J. Wang, M. Luo, and D. Zhang, "A GPU-accelerated approach for collision detection and tool posture modification in multi-axis machining," *IEEE Access*, vol. 6, pp. 35132–35142, 2018.

[14] O. Gienke, Z. Pan, L. Yuan, T. Lepper, and S. Van Duin, "Mode coupling chatter prediction and avoidance in robotic machining process," *Int. J. Adv. Manuf. Technol.*, vol. 104, nos. 5–8, pp. 2103–2116, Oct. 2019.

[15] A. Brunete, E. Gambao, J. Koskinen, T. Heikkilä, K. B. Kaldestad, I. Tyapin, G. Hovland, D. Surdilovic, M. Hernando, A. Bottero, and S. Anton, "Hard material small-batch industrial machining robot," *Robot. Comput.-Integr. Manuf.*, vol. 54, pp. 185–199, Dec. 2018.

[16] Z.-L. Xu, S. Lu, J. Yang, Y.-H. Feng, and C.-T. Shen, "A wheel-type in-pipe robot for grinding weld beads," *Adv. Manuf.*, vol. 5, no. 2, pp. 182–190, Jun. 2017.
[17] O. Rovný, G. Batista, G. Takács, J. Vachálek, and P. Blažíäek, "Automatic machining system for the refurbishment of degraded welds in piping systems," *Adv. Mech. Eng.*, vol. 9, no. 11, Nov. 2017, Art. no. 168781401773798.
[18] V. Pandiyan, P. Murugan, T. Tjahjowidodo, W. Caesarendra, O. M. Manyar, and D. J. H. Then, "In-process virtual verification of weld seam removal in robotic abrasive belt grinding process using deep learning," *Robot. Comput.-Integr. Manuf.*, vol. 57, pp. 477–487, Jun. 2019.
[19] V. Pandiyan, W. Caesarendra, T. Tjahjowidodo, and H. H. Tan, "In-process tool condition monitoring in compliant abrasive belt grinding process using support vector machine and genetic algorithm," *J. Manuf. Processes*, vol. 31, pp. 199–213, Jan. 2018.
[20] V. Pandiyan and T. Tjahjowidodo, "In-process endpoint detection of weld seam removal in robotic abrasive belt grinding process," *Int. J. Adv. Manuf. Technol.*, vol. 93, nos. 5–8, pp. 1699–1714, Nov. 2017.
[21] V. Pandiyan, W. Caesarendra, T. Tjahjowidodo, and G. Praveen, "Predictive modelling and analysis of process parameters on material removal characteristics in abrasive belt grinding process," *Appl. Sci.*, vol. 7, no. 4, p. 363, 2017. p. app7040363
[22] W. Fan, G. Hou, W. Wang, and Y. Wu, "Dynamic analysis of a novel rail-grinding car using open-structured abrasive belt for high-speed railways," *Math. Problems Eng.*, vol. 2019, pp. 1–9, May 2019, Art. no. 1748679.
[23] W. G. Fan, G. Y. Hou, W. X. Wang, X. L. Zhang, and J. D. Wang, "Design and dynamic analysis of a new rail grinding device using closed abrasive belt," *Int. J. Simul. Model.*, vol. 18, no. 3, pp. 531–542, Sep. 2019.
[24] X. Xu, D. Zhu, H. Zhang, S. Yan, and H. Ding, "Application of novel force control strategies to enhance robotic abrasive belt grinding quality of aero-engine blades," *Chin. J. Aeronaut.*, vol. 32, no. 10, pp. 2368–2382, Oct. 2019.
[25] Z. He, J. Li, Y. Liu, and J. Yan, "Investigation on wear modes and mechanisms of abrasive belts in grinding of U71Mn steel," *Int. J. Adv. Manuf. Technol.*, vol. 101, nos. 5–8, pp. 1821–1835, Apr. 2019.
[26] W. Fan, Y. Liu, X. Song, J. Cheng, and J. Li, "Influencing mechanism of rubber wheel on contact pressure and metal removal in corrugated rail grinding by abrasive belt," *J. Manuf. Sci. Eng.*, vol. 140, no. 12, Dec. 2018, Art. no. 124501.
[27] H. Zhe, L. Jianyong, L. Yueming, N. Meng, and F. Wengang, "Investigating the effects of contact pressure on rail material abrasive belt grinding performance," *Int. J. Adv. Manuf. Technol.*, vol. 93, nos. 1–4, pp. 779–786, Oct. 2017.
[28] S. Yan, X. Xu, Z. Yang, D. Zhu, and H. Ding, "An improved robotic abrasive belt grinding force model considering the effects of cut-in and cut-off," *J. Manuf. Processes*, vol. 37, pp. 496–508, Jan. 2019.
[29] T. Zhang, Y. Yu, and Y. Zou, "An adaptive sliding-mode iterative constant-force control method for robotic belt grinding based on a one-dimensional force sensor," *Sensors*, vol. 19, no. 7, p. 1635, 2019.
[30] X. Zhang, H. Chen, J. Xu, X. Song, J. Wang, and X. Chen, "A novel sound-based belt condition monitoring method for robotic grinding using optimally pruned extreme learning machine," *J. Mater. Process. Technol.*, vol. 260, pp. 9–19, Oct. 2018.
[31] Y. Liu, W. Dai, G. Xiao, and Y. Huang, "Surface integrities of different trajectories in belt grinding for pure iron functional performance test pieces," *Crystals*, vol. 9, no. 3, p. 123, 2019.
[32] Y. Liu, Q. Li, G. Xiao, and Y. Huang, "Study of the vibration mechanism and process optimization for abrasive belt grinding for a blisk-blade," *IEEE Access*, vol. 7, pp. 24829–24842, 2019.
[33] M. Zhang, T. Chen, S. Cao, F. Zheng, and Y. Tan, "A dynamical tool adjustment method for computer numerical control abrasive belt grinding," *Adv. Mech. Eng.*, vol. 11, no. 5, May 2019, Art. no. 168781401984627.
[34] J. Duan, Y. Zhang, and Y. Shi, "Belt grinding process with force control system for blade of aero-engine," *Proc. Inst. Mech. Eng., B, J. Eng. Manuf.*, vol. 230, no. 5, pp. 858–869, May 2016.
[35] B. Hou, Y. Wang, F. Wang, Z. Ji, and H. Liu, "Research on belt grinding for marine propeller blade based on the second-order osculation," *Int. J. Adv. Manuf. Technol.*, vol. 80, nos. 9–12, pp. 1855–1862, Oct. 2015.
[36] J. Wang, D. Zhang, B. Wu, M. Luo, and Y. Zhang, "Kinematic analysis and feedrate optimization in six-axis NC abrasive belt grinding of blades," *Int. J. Adv. Manuf. Technol.*, vol. 79, nos. 1–4, pp. 405–414, Jul. 2015.
[37] C. Bi, X. Hao, and J.-G. Fang, "Establishment and realization of intelligent integrated grinding and measuring workcell for blade edges," *J. Chin. Soc. Mech. Eng.*, vol. 40, pp. 149–159, May 2019.
[38] T. Zhang and J. Su, "Collision-free planning algorithm of motion path for the robot belt grinding system-2018," *Int. J. Adv. Robot. Syst.*, vol. 15, pp. 149–159, Dec. 2018.
[39] S. Han, X. Zhao, Q. Fan, and B. Tao, "Automatic programming for dual robots to grinding intersecting curve," in *Proc. 12th Int. Conf., Intell. Robot. Appl. (ICIRA)*, Shenyang, China, 2019, pp. 508–516.
[40] M. Tognon, H. A. T. Chavez, E. Gasparin, Q. Sable, D. Bicego, A. Mallet, M. Lany, G. Santi, B. Revaz, J. Cortes, and A. Franchi, "A truly-redundant aerial manipulator system with application to Push-and-Slide inspection in industrial plants," *IEEE Robot. Autom. Lett.*, vol. 4, no. 2, pp. 1846–1851, Apr. 2019.
[41] W. Gao, Q. Tang, J. Yao, and Y. Yang, "Automatic motion planning for complex welding problems by considering angular redundancy," *Robot. Comput.-Integr. Manuf.*, vol. 62, Apr. 2020, Art. no. 101862.
[42] T. Zhang, S. Chen, M. Wu, Y. Zhao, and X. Chen, "Optimal motion planning of all position autonomous mobile welding robot system for fillet seams," *IEEE Trans. Autom. Sci. Eng.*, vol. 10, no. 4, pp. 1147–1151, Oct. 2013.
[43] T. Zhang, M. Wu, Y. Zhao, and S. Chen, "Motion planning for a new-model obstacle-crossing mobile welding robot," *Ind. Robot. Int. J.*, vol. 41, no. 1, pp. 87–97, Jan. 2014.
[44] T. Zhang, M. Wu, Y. Zhao, X. Chen, and S. Chen, "Optimal motion planning of mobile welding robot based on multivariable broken line seams," *Int. J. Robot. Autom.*, vol. 29, no. 2, pp. 215–223, 2014.

WANJIN GUO received the B.S. degree in mechanical and automation engineering from Chang'an University, Xi'an, China, in 2007, the M.S. degree in mechatronic engineering from Xidian University, Xi'an, in 2010, and the Ph.D. degree in mechatronic engineering from the Harbin Institute of Technology, Harbin, China, in 2017.

He is currently an Assistant Professor with Chang'an University. His research interests include industrial robotics and applications, robotic grinding, robotic deburring, hybrid robot manipulator, motion planning and motion control, and machine vision.

YAGUANG ZHU (Member, IEEE) received the B.S. degree in mechanical and automation engineering from Shandong University, Jinan, China, in 2009, and the Ph.D. degree in mechatronic engineering from Zhejiang University, Hangzhou, China, in 2014.

He is currently a Professor with Chang'an University, Xi'an, China. His research interests include legged robots, parallel robot, bio-inspired control, pattern recognition, and electro-hydraulic control systems. He is a member of the Chinese Association of Automation and International Society of Bionic Engineering. He is an Editor of the *International Journal of Robotic Engineering*.

XU HE received the B.S. degree in mechanical and automation engineering from the Xi'an University of Architecture and Technology, Xi'an, China, in 2018. He is currently pursuing the M.S. degree in mechanical engineering with Chang'an University, Xi'an.

His research interests include industrial robotics, robotic grinding, and mechatronics.